Colloids and Surfaces A 529 (2017) 146–159

Contents lists available at ScienceDirect

Colloids and Surfaces A

journal homepage: www.elsevier.com/locate/colsurfa

# Cerium oxide nanoparticles: Synthesis, characterization and tentative mechanism of particle formation

Jazmín Calvache-Muñoz, Fabiola A. Prado, Jorge E. Rodríguez-Páez*

*Research Group CYTEMAC, Department of Physics, University of Cauca, Popayan, Colombia*

## GRAPHICAL ABSTRACT

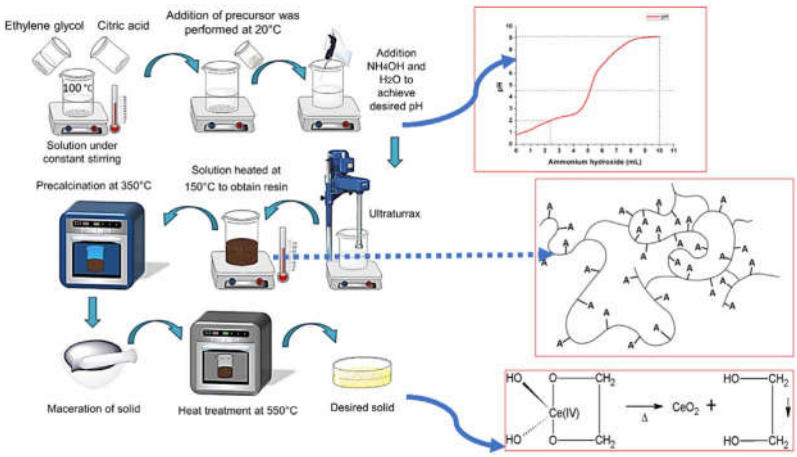


## ARTICLE INFO

*Keywords:*
Ceria-NPs
Synthesis
Characterization
Mechanism of formation

## ABSTRACT

Given the scientific and technological interest in cerium oxide (ceria), in this paper nanoparticles of ceria (ceria-NPs) were synthesized using a modified polymer complex process (modified Pechini), while varying the pH of the system. This methodology made it possible to obtain, in a reproducible and controlled way, nanoparticles of ceria (< 100 nm) of a high chemical purity at low temperatures. The precalcined cerium solid obtained at 350 °C was characterized using differential thermal analysis (DTA), thermogravimetric analysis (TG) and IR spectroscopy. Very little organic phase was found in the respective spectra, indicating that the inorganic phase, cerium oxide, is predominant. Carbonaceous residues still present in the solids were removed by heating at temperatures above 500 °C and the samples obtained were characterized using X-ray diffraction (XRD), IR, UV–vis absorption and diffuse reflectance spectroscopies, and Transmission Electron Microscopy (TEM). The diffractograms of the samples showed that the only crystalline phase present was $CeO_2$. From the results of UV-vis absorption and diffuse reflectance spectroscopy, two important energy values were obtained, 3.8 eV and 3.4 eV. These could be attributed to the energy gap value (3.8 eV) and to a possible "mid-gap" (3.4 eV). Furthermore, on increasing the synthesis pH, a reduction in particle size results, the particle being between 10 and 20 nm, with a spheroidal shape. By looking at the different stages of the synthesis process, a mechanism is proposed to explain how nanoparticles of ceria are formed.

* Corresponding author.
*E-mail addresses:* jnpaez@unicauca.edu.co, jnpaez60@yahoo.com (J.E. Rodríguez-Páez).

http://dx.doi.org/10.1016/j.colsurfa.2017.05.059
Received 4 March 2017; Received in revised form 17 May 2017; Accepted 20 May 2017
Available online 25 May 2017
0927-7757/ Published by Elsevier B.V.

## 1. Introduction

Given the current importance of nanotechnology, nanoparticles are of immense interest due to their scientific and technological significance. This is because of special properties they exhibit that their bulk counterparts do not [1,2]. As a result of these novel properties, nanoparticles have multiple applications, including catalysts [3,4], drug delivery [5], antibacterial [6], electronics, optoelectronics, plasmonics, information storing, optical sensing, bio-imaging and biomedicine [2,7,8]. Specifically, nanoparticles have the advantage, when applied in life science and the environment, that their size is comparable with the dimensions of small molecules (~1–10 nm) or viruses (~10–100 nm), which allows them to attack biological entities without changing their functions. In the environment, the small size of the particles, together with their large surface area, enables them to detect specific contaminants, from the presence of which pollution often arises. In addition, nanoparticles can actively interact with a pollutant and treat it [9].

Furthermore, looking specifically at cerium, it is very reactive in the presence of atmospheric oxygen, generating stable oxides [10] that vary in composition and are commonly known as ceria. Bulk cerium oxide has at least two stable stoichiometrics, the dioxide ($CeO_2$) and dicerium trioxide ($Ce_2O_3$), commonly referred to as sesquioxide [11,12]. Pure $CeO_2$ has a fluorite-type structure, with a special *Fm3m* group, especially in the temperature range from room temperature to melting point. $CeO_2$-$Ce_2O_3$ phase transition depends on the oxygen pressure in the system and on temperature [11,13], a transition of reduction that can be attributed to the formation and migration of oxygen vacancies, a process that can be linked to a quantum process of ionization/delocalization of the 4f electrons of cerium, as proposed by Skorodumova et al. in their work [14]. The close thermodynamic stability of $CeO_2$ and $Ce_2O_3$ favors an easy and reversible transition between these two compounds, giving rise to a range of partially reduced $CeO_{2-x}$ phases that serve as oxygen reservoirs by creating or eliminating oxygen vacancies. The study of these intermediate phases has been going on since the mid-twentieth century [15,16], driven by technological developments that have been made, utilizing the capacity of ceria for oxygen storage. It is worth noting that undesirable properties are also evident, such as chemical expansion with increasing temperature, on changing the concentration of oxygen vacancies [17].

The formation of a single oxygen-vacancy is an elementary process in the reduction of $CeO_2$ to $Ce_2O_3$. With the formation of the oxygen vacancies, an increase in the $Ce^{3+}$ fraction is produced in the structure of the ceria in order to maintain electroneutrality [18]. The valence and defect structures of $CeO_2$ are dynamic and can change spontaneously or in response to physical parameters such as temperature, partial oxygen pressure, doping with other ions, and on applying an electric field or surface stress [12]. The energy cost of forming an oxygen vacancy in ceria (387 ± 13 KJ/mol [19,20]), is relatively low considering the energy involved in the reduction of $CeO_2$ to $Ce_2O_3$ (~382 KJ/mol [20,21]), where oxygen is released and an oxygen vacancy is formed through the following reaction:

$$O_o^x + 2Ce_{Ce}^x \leftrightarrow V_o^{\cdot\cdot} + 2\,Ce_{Ce}^{'} + \tfrac{1}{2}O_2(g) \quad (1)$$

Considering the above reaction, the formation of the oxygen defect would be accompanied by the localization of the electrons left behind in Ce 4f states, leading to the formation of two $Ce^{3+}$. Although it was long considered that the cations of Ce in the nearest neighbor position to the oxygen defect become reduced, recent computations indicate that the $Ce^{3+}$ resulting from formation of an oxygen vacancy is located at sites farther away from the vacancy position [22]. This process would be possible due to the ability of the cerium atom to facilitate and adjust its electronic configuration to best fit with its immediate environment so that the formation of the oxygen vacancy would be linked closely to the quantum effect of localization/delocalization of the 4f electrons of cerium, an action that would be the basis for explaining the oxygen storage capacity of the cerium oxide [14]. The formation of reduced oxides can be viewed upon as a formation, migration, and ordering of virtual $Ce^{3+}$-vacancy complexes [14,23].

The wide technological application of ceria is due mainly to the capacity to store and release oxygen in its intrinsic n-type fluorite structure, i.e. its ability to repeatedly pass through redox cycles rapidly. This behavior would be related to the ease of forming and repairing oxygen vacancies at the solid ceria surface [20]. These unique redox properties have opened up new and promising applications for ceria in the area of catalysis [21,24], production and purification of hydrogen [25] and removal of CO from vehicle exhaust [26]. Because of the mobility of oxygen vacancies, which favors high ionic conductivity, ceria is considered as a promising electrolyte for solid oxide fuel cells [27]. Furthermore, due to the electronic structure of ceria, it can be used as a UV absorber in the cosmetics industry and in the manufacture of window glass, as well as in light harvesting devices and optical displays [28]. Ceria also plays an important role in the treatment of toxic emissions, removal of soot from diesel engine exhaust and organic molecules from wastewater [29], in biomedicine [30], as an oxygen sensor [31], in pharmacology [32] and for degrading inks [33].

The behavior of ceria, its redox properties for example, is closely related to its crystalline structure, which depends on the synthesis process used to obtain it [12]. Review articles are found in the scientific literature on obtaining ceria [10,12,34,35], highlighting the methods of hydrolysis [36], thermal deposition [37], sol-gel[38], combustion [39], hydrothermal and solvothermal [40,41], microemulsion [42], sonochemical synthesis [43] mechanochemical [44] and precipitation [45,46], among others.

The production of Ce materials with a good performance at an industrial level is necessary to be able to understand the chemical activity of the oxide, which depends mainly on its electronic structure that, at the nanoscale level, is affected by particle morphology. At this size scale, the chemical activity of ceria increases, mainly due to the formation of vacancies and to the increase of the surface to bulk ratio [12,47]. This has led researchers to conduct studies on the control of the morphology and size of the ceria through the synthesis process [12,24,35,48], by using surfactants [49,50] and controlling certain synthesis parameters such as temperature [51], the acidic or basic character of the system [52], and the nature of the solvent of synthesis [53,54], among others. Knowing and understanding the processes of synthesis of ceria would make it possible to control its final structure, both at surface and bulk level, and therefore the properties of the product.

The nanoparticles of $CeO_2$ ($CeO_2$-NPs) are special because their physicochemical properties, and therefore their functionality, are defined by the synthesis method used. In their paper, Karakoti et al. [55] showed that the methods of synthesis of ceria and its processing history may signicantly impact particle behavior. This is why to understand and predict the behavior of nanoparticles it is necessary to guarantee the reliability and reproducibility of the production methods. Although many stages of the synthesis process are well understood and reproducible in the hands of experienced researchers, the results of Karakoti et al. [55] indicate that small and apparently insignificant differences could strongly alter the properties of the final product or its aging process. In general, it is assumed, for example, that toxicity is increased on reducing the size of the nanoparticles [56,57] which for the specific case of nanoceria would imply a large surface area:volume ratio that would favor a large surface $Ce^{3+}/Ce^{4+}$ ratio and hence the higher toxicity for the smaller $CeO_2$-NPs [58]. But this is not always so. Studies with large particles of ceria showed that their toxicity differed little or not at all from that of nanoparticles toward eukaryotic cells [59]. Kumar et al. [60] noticed that small modifications in the synthesis process could have a major impact on the biological activity and toxicity of ceria, and in general on its functionality, so reproducibility in nanomaterial synthesis often constitutes a challenge. These

investigators [60] indicated that it was necessary to determine what would be the most appropriate way to synthesize $CeO_2$-NPs for relevant environmental/toxicology/safety studies. For this, it is necessary to take into account, as indicated by Reed et al. in their work [61] that, since not all $CeO_2$-NPs are synthesized in the same way, their toxicological profiles are expected to be different. This leads to the need to determine what the synthesis parameters, particle size, stabilizers and other chemistries are that would affect these profiles. Considering the above, present work and its results are of interest since, in addition to describing the synthesis method and making an adequate characterization of the obtained product, it proposes a tentative mechanism to explain the different stages of formation of the nanoparticles. Knowing tentatively the mechanism of formation of the particles, the properties of the final product could be affected in a predetermined and favorable way.

It is thus necessary to control the synthesis process very closely to manipulate the shape, exposed crystal planes and particle size of the ceria required in its many technological applications. Particular attention must be paid to the mechanisms of particle formation to establish synthesis strategies, morphological manipulation, and assembly behaviors of the nano-building blocks [62]. In the work of Hsu et al. [63] the purpose of knowing the effect of some synthesis parameters for controlling the shape and size of the particles obtained is evident. They synthesized cerium (IV) oxide nanoparticles with a narrow size distribution, starting from the hydrolytic deprotonation of cerium (IV) ions in the presence of dilute sulfuric acid. The results of the research indicated that the morphology of the particles was altered by the concentration of the reactants and the nature of the anions in solution. They obtained spherical particles of ceria at low concentrations of cerium sulfate and $H_2SO_4$ and, depending on the acidity of the aging time, the diameter of the particles ranged from 30 to 240 nm. Another work in which the mechanism of formation of ceria nanoparticles was discussed is that of Zhang et al. [54]. They used the solvothermal method to obtain ceria nanospheres using a mixture of water and diethylene glycol as the reaction solvent with the aid of polyvinylpyrrolidone (PVP). From the results of their research they concluded that the surfactant and the solvent of synthesis are determining factors in the mechanism of formation of the nano-spheres and that adjusting the reaction temperature and time could control their size. In the feature article of Yuan et al. [62] a careful description of various methods of synthesis for obtaining ceria-based nanomaterials was carried out, highlighting the effect that some of the critical parameters of synthesis have on the size and shape of the particles obtained, as well as the high sensitivity of these processes of synthesis to the nature of the solvent or surfactant, pH gradients, environmental conditions (temperature, pressure and humidity), contaminants, time, etc.

In this work, nanoparticles of ceria (ceria-NPs) were synthesized using a modified polymer complex process (modified Pechini), varying the pH of the system, a methodology made it possible to obtain ceria nanoparticles in a controlled and reproducible way with high chemical purity at low temperatures. The solids obtained were characterized using DTA/TG, FTIR spectroscopy, X-ray diffraction (XRD), UV–vis absorption spectroscopy and diffuse reflectance and transmission electron microscopy (TEM). Considering the different stages of the synthesis process used, a tentative mechanism was proposed to explain the formation of the ceria-NPs.

## 2. Experimental procedure

### 2.1. Cerium oxide synthesis

#### 2.1.1. Formation of resin

To synthesize the ceramic powders of the $CeO_2$ system, using the modified Pechini method, hydrated cerium nitrate (Alfa Aesar, 99.5%) was used as precursor. To obtain 5 g of cerium oxide, 12.6 g of precursor was used in a mixture of citric acid (CA − Merck 99.5%) and ethylene glycol (EG − Mallinckrodt 99.8%) in a 1: 4 mass ratio (13.5 mL of ethylene glycol and 4 g citric acid), a mixture that was heated to a temperature of 100 °C, maintaining it in continuous and constant agitation to favor the dissolution of the citric acid in the polyol. After 30 min of heating the system. it was allowed to cool and the precursor proceeded to be added, the 12.6 g of hydrated cerium nitrate ($Ce(NO_3)_3{\cdot}6H_2O$) dissolved in 40 mL of water, maintaining the agitation of the system to guarantee a homogeneous mixture. It must be ensured that the solution, a result of the previous process, is completely transparent, a condition that guaranteed a uniform mixing of the different reagents and the homogeneous formation of the citrate.

Subsequently, ammonium hydroxide $NH_4OH$ (Merck 25%) was added to the obtained solution at a delivery rate of 0.1 mL/s using a meterer (Metrohm Dosimat 685), and the system was brought to a higher pH value (which was called working pH) ensuring that the solution remained transparent; simultaneously, water was gradually added to the solution until a total volume of 220 mL was obtained, independent of the working pH value. A strict control was maintained over the pH changes to avoid the formation of precipitates, observing that for pH values above 2.5 a solid phase formed within the system. This mixture was subjected to the action of a high shear equipment (Ultraturrax T50) to eliminate the presence of the precipitates that had been formed during the process. For the other sample, synthesized at pH ~9.2, more $NH_4OH$ was added to the solution until this pH value was reached, ensuring total transparency of the solution. To guarantee the reproducibility of the synthesis process, the variation in pH of the solution was recorded during the addition of $NH_4OH$. The solution obtained, independent of the pH value, was then heat treated at a temperature of 150 °C, for 3 h, under constant stirring, to favor the polyesterification reactions and therefore the formation of the resin.

#### 2.1.2. Synthesis of ceramic powders

On obtaining the resin, it was subjected to a pre-calcination process at a temperature of 350 °C in an oven (HACEB model HL40) for 2 h to give a pale yellow powder with a low carbon content such as was indicated by the IR spectroscopy tests performed on these samples. The final heat treatment was carried out following a pre-structured heating program which involved a first treatment at 150 °C for 30 min and then at 550 °C for 3 h to remove the remaining organic material.

### 2.2. Characterization of ceramic powders

Various characterization techniques were used to determine the characteristics of the synthesized solids.

#### 2.2.1. Thermal analysis

In order to determine the effect of the heat treatments on the samples obtained and to define the most appropriate temperature at which the sample should be subjected to obtain the oxide of interest, differential thermal analysis (DTA) and thermogravimetric analysis (TGA) tests were carried out using the Thermogravimeter SDT Q600 – TA Instruments, at a heating rate of 5 °C/minute.

#### 2.2.2. Fourier transform infrared spectroscopy (FTIR)

In this work the technique of infrared spectroscopy was used in order to determine the functional groups present in the samples and the effect on them of the different chemical and thermal treatments to which the synthesized solids were submitted. For this purpose, the Thermo Scientific ™ Nicolet ™ iS ™ 10 FT-IR spectrometer spectrophotometer was used.

#### 2.2.3. X-ray diffraction (XRD)

The crystalline structure of the ceria samples synthesized in this work was identified using the X-ray diffractometer − Pro PANalytical X'Pert X-ray using the $K_\alpha$ radiation of Cu ($\lambda = 1.5418740\,\dot{A}$), in a Bragg-Bretano configuration. The powder samples were analyzed in the range

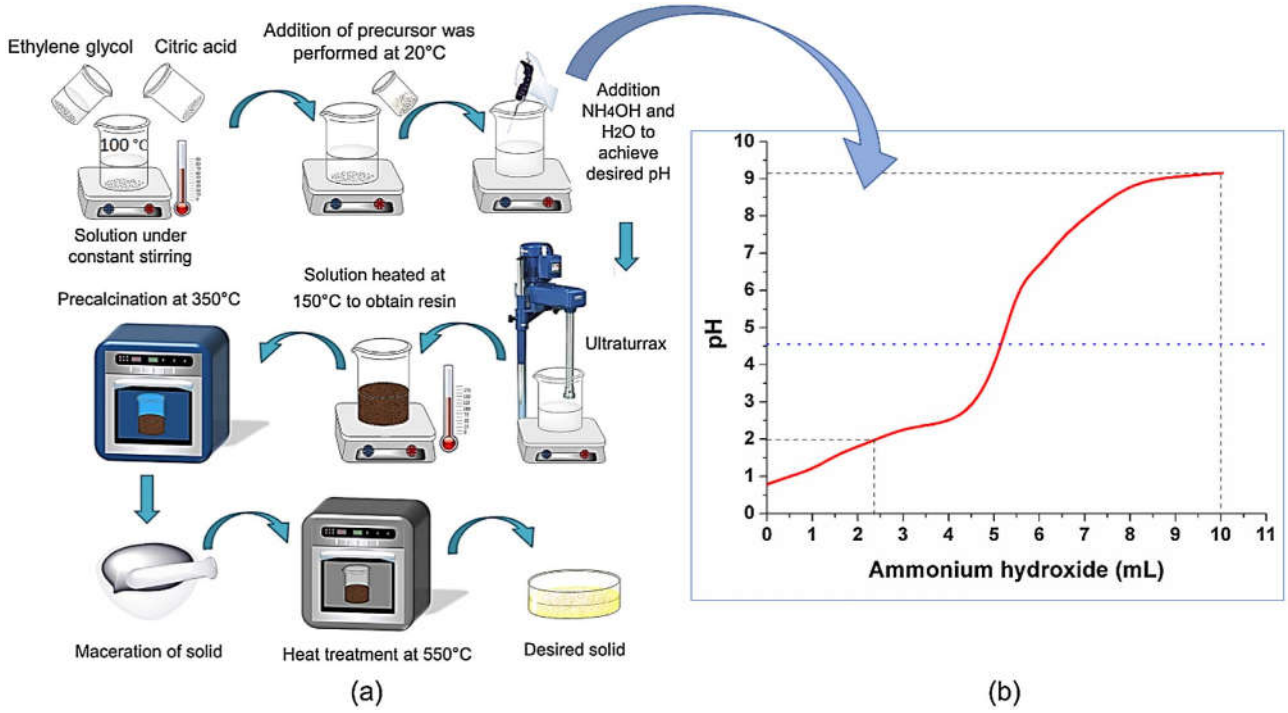


**Fig. 1.** (a) Diagram of modified Pechini method used to obtain $CeO_2$ powders and (b) Potentiometric titration curve of the cerium system.

between 20 and 100°, with a step of 0.004 and a time per step of 90 s.

The Scherrer formula was used to obtain the average crystallite size, using the most intense peak of the diffractogram, a formula given by [64]:

$$\tau = \frac{K\lambda}{\beta Cos\theta} \tag{2}$$

where $\tau$ is the mean crystallite size, K is a dimensionless form factor (in this work the value of 0.9 was used), λ is the wavelength of the incident X-rays, β the width at the mean peak height (FWMH) and θ the diffraction angle. To determine the network constants, Rietveld refinement was employed, using the MAUD program.

### 2.2.4. Ultraviolet-visible absorption spectroscopy (UV–vis)

The absorption of ultraviolet and visible radiation was used to determine the most important electronic transitions caused by the incidence of UV–vis radiation and that causes the excitation of the bonding electrons. In this case, as with the ion spectra of the lanthanide and actinide series, the electrons responsible for the absorption of these elements are the 4f and 5f, respectively.

The absorption spectra of the samples of cerium oxide synthesized in this work were taken with a Thermo Scientific Genesys 6 UV–vis, in the range of wavelengths between 200 and 900 nm, using quartz cuvettes of 1 cm in length. The ceria powders were macerated in an agate mortar to then take a sample of approximately 2.0 mg, which was dispersed in 20 mL of distilled water. This suspension, with a concentration of ~100 ppm, was sonicated for 15 min. Subsequently, absorption spectra were taken of the samples of interest.

### 2.3. Ultraviolet-visible spectroscopy of diffuse reflectance

This technique makes it possible to obtain, from the UV–vis diffuse reflectance spectra, the energy gap value of a semiconductor solid using the following equation [65]:

$$\alpha_b = \frac{B(h\nu - Eg)^n}{h\nu} \tag{3a}$$

and using the Kubelka-Munk model [66]:

$$[F(R_\infty)h\nu] = B(h\nu - Eg)^n \tag{3b}$$

with:

$$F(R_\infty) = \frac{(1 - R_\infty)^2}{2R_\infty};\ R_\infty = \frac{R_{Sample}}{R_{standart}} \tag{3c}$$

The terms of the equation correspond to: $\alpha_b$ absorption coefficient, $h\nu$ absorbed energy, B absorption constant, $Eg$ energy gap energy, $F(R_\infty)$ Kubelka-Munk function, R reflectance, n constant with values ½ (direct transition) or 2 (indirect transition), which in the case of ceria is a direct transition (n = ½). When the value $\alpha_b$, absorption coefficient, takes zero or $F(R_\infty)$ is zero, applying equation 3a or 3b, respectively, the energy absorbed is equal to the energy of the gap. Therefore, by representing $(\alpha_b h\nu)^2$ or $[F(R_\infty)h\nu]^2$ as a function of $h\nu$, a line can be obtained at the absorption edge, tangent to the curve represented, and if it is extrapolated, to cut the energy axis, the cutting point would make it possible to obtain the energy value of the gap. The diffuse reflectance spectrum of the predetermined ceria samples were recorded using the JASCO V-670 UV-vis-NIR spectrophotometer in the wavelength range of 200–800 nm at a scanning speed of 100 nm/min.

### 2.3.1. Transmission electron microscopy (TEM)

In this work TEM was used to determine the size and morphology of the particles of the samples obtained, using the Jeol JEM1200EX electron microscope of the Electron Microscope Unit, UME, of the University of Cauca.

## 3. Results and discussion

The diagram of the synthesis process used to obtain the cerium oxide is illustrated in Fig. 1(a). Fig. 1(b) shows the potentiometric titration curve obtained during the process of addition of $NH_4OH$ to the system, a curve that can be used as a reference to ensure the reproducibility of the process; in it the different stages of the process are observed and the values of the working pH are indicated: ~0.8, ~2 and ~9.

Fig. 2 shows the ATG/ATD curves corresponding to the solid previously treated at 350 °C. It can be seen that the sample did not show an

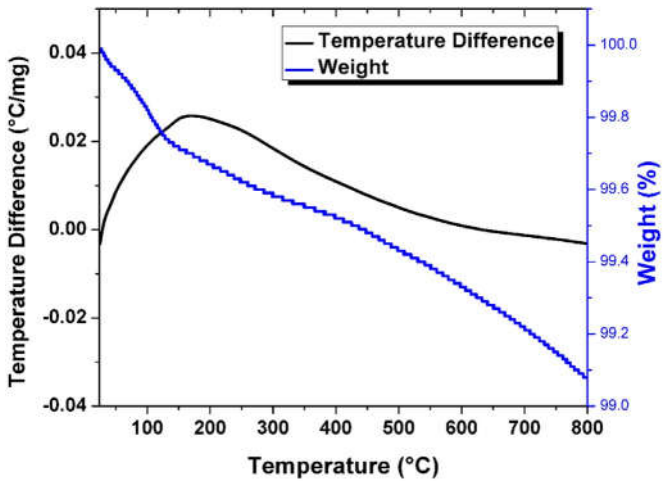


**Fig. 2.** DTA/TGA curves, in air, corresponding to the solid synthesized and heat treated at 350 °C.

appreciable loss of weight, only 1% of the total weight up to 800 °C. The weight loss between room temperature and 100 °C, approximately 0.4%, can be associated with the evaporation of the physisorbed water on the surface of the solid, so subtle that the corresponding endothermic peak is not evident in the ATD curve. The additional loss, 0.6%, can be attributed to the oxygen output of the samples. The change in the baseline of the ATD curve, between ambient temperature and 150 °C, would indicate a subtle change in the thermal capacity of the solid. From 150 °C to 800 °C, there is a slight exothermic behavior that could be associated with the exit of the oxygen, which would favor the formation of the different non-stoichiometric $CeO_{2-x}$ phases, as indicated by the phase diagrams of the Ce-O system[10,67–69]. Overlapping this behavior of the ATD curve, in this temperature range, there may also be a change in the baseline associated with the variation of the thermal capacity of the sample.

### 3.1. IR spectroscopy of samples synthesized at different pH values

Fig. 3 shows the IR spectra, in the range of 4000–400 $cm^{-1}$, taken from the powders synthesized by the modified Pechini method obtained at different working pH values, without (Fig. 3(a)) and with heat treatment (Fig. 3(b)) after the resin precalcination process. All spectra showed a large band around the 400–630 $cm^{-1}$, an absorption band that can be attributed to the vibrational mode of tension of the Ce—O [70–72], corresponding to the active $F_{1U}$ mode in the IR for the fluorite structure, which would confirm the presence of ceria in the solid [72,73]. In addition, a large band around 3450 $cm^{-1}$ is present, which can be associated with the vibrational tension mode of the O—H [74] corresponding to residual water and/or hydroxyl groups. The bands around 1300 and 950 $cm^{-1}$ might correspond to the vibrational stretching mode of $H_2O$ [71,75,76], bands that are attenuated after the treatment at 550 °C, the band corresponding to the synthesized $CeO_2$ being that of the lowest intensity at pH 2. The band at ~1625 $cm^{-1}$ may be associated with H—O—H flexion that overlaps with the band corresponding to the O—C—O stretching [74,76], which varies in intensity following calcination or on modifying the synthesis pH.

It should be noted that the absorption bands located in the 2300–3000 $cm^{-1}$ region can be attributed to the hydrocarbon (C—H) stretching modes and are present in all IR spectra. As reported by Vantomme et al. [76] and Chen et al. [77], these bands show the reactivity of ceria with these species, at the surface level, a higher reactivity being observed for the samples synthesized at acid pH.

In the regions ~2340–2370 and 1000–1500 $cm^{-1}$ the bands associated with carbonate-type species related to the surface of the oxide particles, such as atmospheric $CO_2$ for example, which interact with the cerium cations [74,77,78] generating species that would decompose after treatment of the solid at high temperatures [64,71]. As can be seen in Fig. 3, the oxides synthesized at very acid (~1) and basic (9.14) pH values show a high reactivity with the atmosphere if they have not been thermally treated at high temperatures (Fig. 3(a)), a behavior that decreases for the sample synthesized at pH ~2. In the IR spectra in Fig. 3, a small band at 1060 $cm^{-1}$ is observed that may be attributed to stretching vibrations of the Ce—O—C [71].

Fig. 4 shows the major bands of the deconvolved spectrum, in the 400–1000 $cm^{-1}$ range, of the solids synthesized at different pH values precalcined ("without HT") or treated at 550 °C/3 h ("with HT"), a region where the characteristic bands associated with the bonds of cerium with oxygen are found. The location of these bands is summarized in Table 1. Observing Fig. 4, and Table 1, the band around 388 $cm^{-1}$ is characteristic of the synthesized cerium compounds, exhibiting a slight shift towards high wave numbers, both on increasing the pH of synthesis and heat treating the solids. The bands located at ~494 and ~550 $cm^{-1}$ were present in all the IR spectra (Fig. 4) and can be associated with the vibrational stretching mode of Ce—O [79,80]. The IR spectra of the heat treated samples showed a band at ~ 714 $cm^{-1}$ which could be attributed to the enveloping of the phonon band of the metal oxide network [81,82].

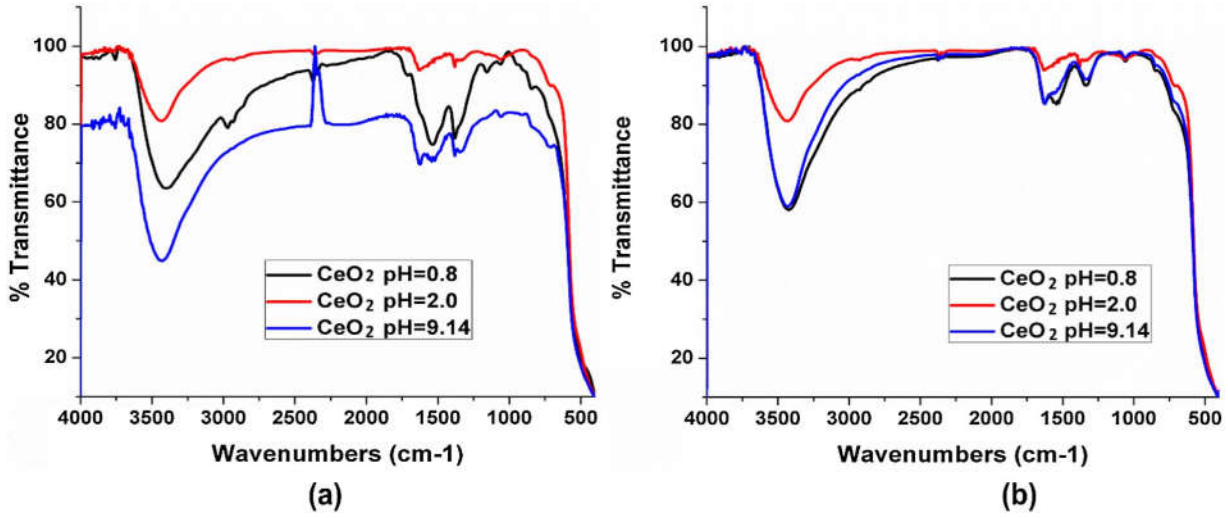


**Fig. 3.** IR spectra corresponding to powders obtained at different pH values of synthesis: (a) without heat treatment (precalcined at 350 °C) and (b) treated at 550 °C/3 h.

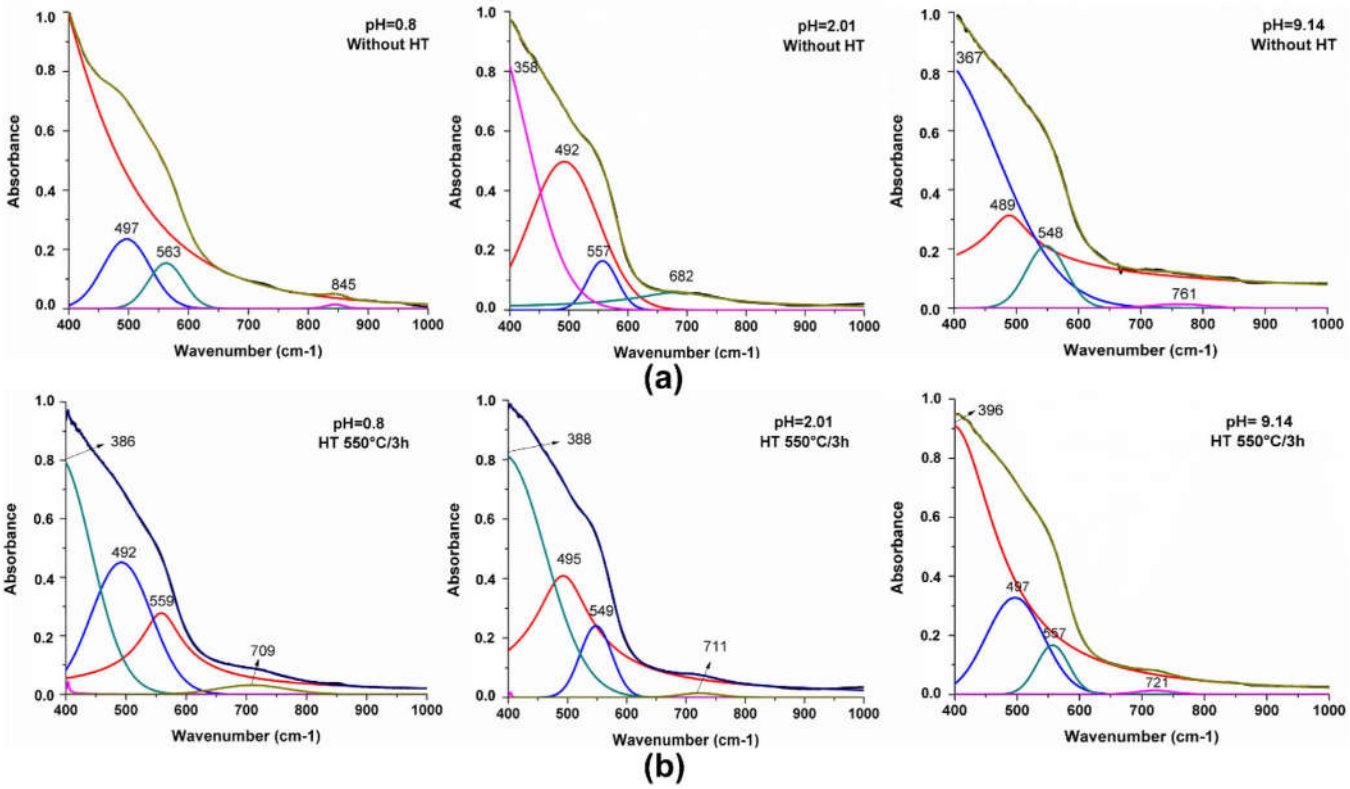


**Fig. 4.** Deconvolution of the IR spectra in the 400–1000 $cm^{-1}$ range corresponding to solid samples of cerium compounds synthesized at pH 0.8, ~pH 2 and pH 9.14 (a) precalcinated (without HT) and (b) treated at 550 °C/3 h (HT).

**Table 1**
Bands in IR spectra in the 400–1000 $cm^{-1}$ range, corresponding to solid samples of cerium compounds obtained at different pH values precalcined (without HT) and treated at 550 °C (with HT).

| $CeO_2$ – without HT. pH ~ 1 | $CeO_2$ – with HT. pH ~ 1 | $CeO_2$ – without HT. pH ~ 2 | $CeO_2$ – with HT. pH ~ 2 | $CeO_2$ – without HT. pH = 9.14 | $CeO_2$ – with HT. pH = 9.14 |
|---|---|---|---|---|---|
| $\upsilon(cm^{-1})$ | $\upsilon(cm^{-1})$ | $\upsilon(cm^{-1})$ | $\upsilon(cm^{-1})$ | $\upsilon(cm^{-1})$ | $\upsilon(cm^{-1})$ |
| 220 | 386 | 358 | 388 | 367 | 396 |
| 497 | 492 | 492 | 495 | 489 | 497 |
| 563 | 559 | 557 | 549 | 548 | 557 |
| 845 | 709 | 682 | 711 | 761 | 721 |

### 3.2. Crystal structure of synthesized ceria

On subjecting the synthesized samples to a heat treatment, 550 °C/3 h, a yellow powder characteristic of ceria was obtained. Fig. 5 shows the X-ray diffractograms corresponding to the powders synthesized at different pH values and treated at 550 °C/3 h.

Observing Fig. 5, it can be seen that the diffraction peaks are well defined and correspond to a fluorite type cubic structure (JCPDS 34-0394). No other phase of the ceria or other crystalline compound was observed in the samples studied. Using Rietveld refinement, it was found that the pure samples had the following network parameters: 5.4093003$\dot{A}$ for $CeO_2$ for that obtained at pH ~1, 5.4140615$\dot{A}$ for that obtained at pH ~2.0 (value close to standard 5.41134$\dot{A}$ (JCPDS 34-0394)), and 5.392175$\dot{A}$ for that synthesized at pH = 9.14.

Calculations made using the Scherrer formula showed that the crystallites had dimensions of the order of Ångstroms as follows: 2.05 Å (synthesis pH ~1), 2.47 Å (~pH 2) and 2.27 Å (pH 9.14). To perform these calculations, we take the diffraction peak (111).

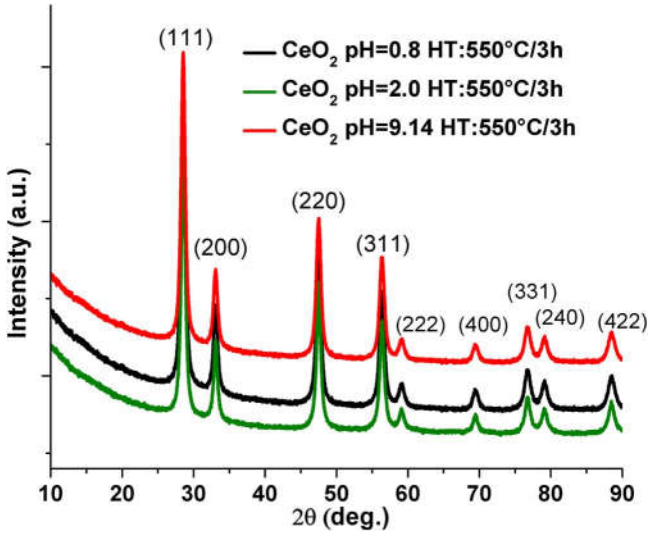


**Fig. 5.** X-ray diffractograms corresponding to the ceria synthesized at different pH values and heat treated at 550 °C/3 h.

### 3.3. UV–vis absorption spectra of the synthesized cerium oxides

Fig. 6(a) shows the UV–vis absorption spectra corresponding to the samples of commercial cerium oxide and those synthesized at pH 0.8, 2.01 and 9.16, subjected to a thermal treatment at 550 °C/3 h. It was observed that the first had a prominent band between 250 nm and 400 nm, with a maximum absorption at 335 nm. For the synthesized oxides, at different pH values, it is observed that the maximum absorption wavelengths occur at 330 nm (pH 0.8), 348 nm (~pH 2) and 330 nm (pH 9.16). The maximum absorption of the ceria synthesized at

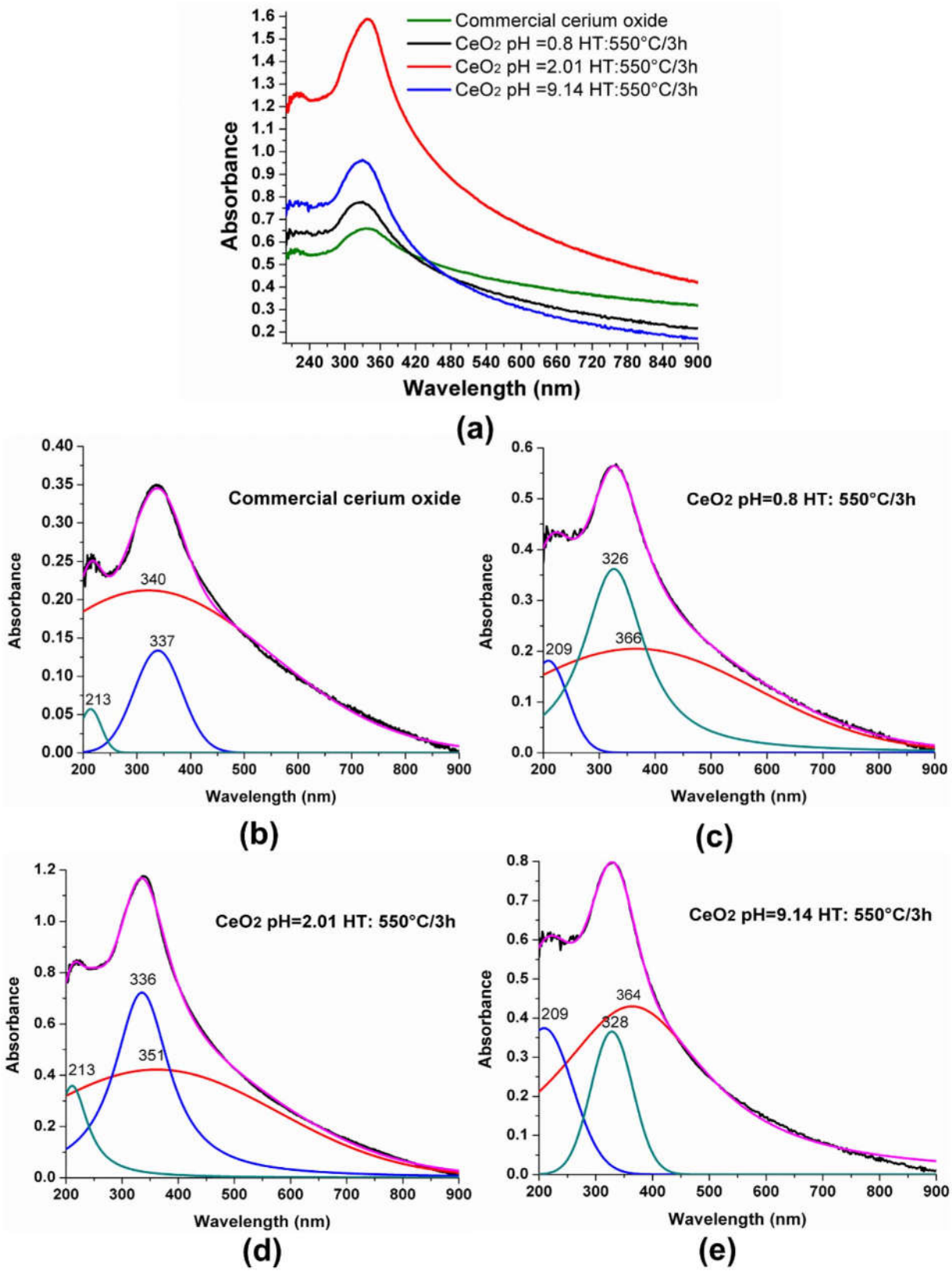


**Fig. 6.** (a) Absorption spectra in the UV–vis corresponding to commercial cerium oxide and those synthesized at different pH and heat treated at 550 °C/3 h, and deconvolutions of these spectra: (b)–(e). Concentration of the sample used for the 100 ppm test.

~pH 2 was maintained in the near ultraviolet, but suffered a slight shift toward the visible.

A mathematical treatment similar to that carried out for the IR spectra (Fig. 4) was performed with the UV–vis spectra in Fig. 6(a). The results of this mathematical modeling are shown in Fig. 6(b)–(e), where the presence is highlighted of three important bands, which make up the respective UV–vis absorption spectrum, for which energy values corresponding to each transition were determined using the equation

**Table 2**
Location of the UV–vis absorption bands and their energy values obtained from the spectra corresponding to the different synthesized $CeO_2$ samples.

| Sample | Wavelength (nm) | Energy (eV) |
|---|---|---|
| Commercial $CeO_2$ | 213 | 5.8 |
| | 337 | 3.7 |
| | 340 | 3.6 |
| $CeO_2$ pH = 0.8 | 209 | 5.9 |
| | 326 | 3.8 |
| | 366 | 3.4 |
| $CeO_2$ pH = 2.01 | 213 | 5.8 |
| | 337 | 3.7 |
| | 351 | 3.5 |
| $CeO_2$ pH = 9.14 | 209 | 5.9 |
| | 328 | 3.8 |
| | 364 | 3.4 |

$E = \frac{h.c}{\lambda}$. Table 2 shows the values obtained on performing these calculations.

The UV–vis absorbance shown by cerium oxide could be accounted for in the main by considering the stoichiometry of the compound [11], a quite controversial issue that has led to different points of view regarding the electronic behavior of ceria [83,84]. Therefore, the activity in the visible spectrum of the synthesized nanoparticles can be attributed both to the unique electronic structure of the ceria, as well as to the presence of defects, mainly oxygen vacancies, and those due to the bi-valence of the Ce.

Regarding its electronic configuration, the way in which the electrons occupy the 4f orbital of Ce has not been clearly defined, because this state is sometimes treated as a part of the interior of the nucleus of $Ce_2O_3$, while in others it is treated as a state of the $CeO_2$ valence band. One of these theories considers that the 4f electron of Ce, in $CeO_2$, is in a mixed valence state, due to the presence of $Ce^{3+}$, a condition that would coexist with the insulating properties of $CeO_2$ by means of a Specific local mixed-valence mechanism between 2p states of oxygen and 4f states of cerium [85,86]. Other authors [87], based on experimental results specifically using X-ray Photoemission Spectroscopy (XPS), concluded that the 4f orbital of the Ce, in the $CeO_2$, would be unoccupied and the Ce ion would be found in the quadrivalent state. Therefore, with respect to the nature of the formation and electronic behavior of $CeO_2$, there are different points of view, depending on the author, and therefore different theories regarding the occupation of the 4f orbitals. Furthermore, because there is no precise information on the optical properties of the sesquioxide ($Ce_2O_3$), specifically on its absorption in the UV–vis, and that the purity of the ceria cannot be guaranteed, there is much uncertainty relating to the UV–vis absorption behavior of $CeO_2$.

Considering the deconvolutions of the UV–vis absorption spectra (Fig. 6), the following energy values corresponding to the respective absorption bands were obtained: 5.8, 3.8 and 3.4 eV, where the last band could be considered as evidence of the presence of energy states in the gap (known as “midgap states”) [88–90]. The absorption band with an energy value of 5.8 eV could be associated to the O 2p − Ce 5d6 s transition; the band corresponding to the value of 3.8 eV could be attributed to the $O^{2-} - Ce^{4+}$ charge transfer, between the bands O 2p and Ce 4f, and the band with energy 3.4 eV could be attributed to the f-d transition in the $Ce^{3+}$ ions isolated in $CeO_2$.

Because the sample with the highest absorbance in the UV–vis was the cerium oxide synthesized at pH ~2, studies were made on this sample of the effect of the heat treatment times and the temperature value. The absorbance curves in Fig. 7 show a marked variation in both the amplitudes and absorption bandwidth as the heat treatment times are modified.

The wavelength at which the maximum absorbance occurs (around 347 nm) varies very little in the samples treated at 550 °C (see Fig. 7),

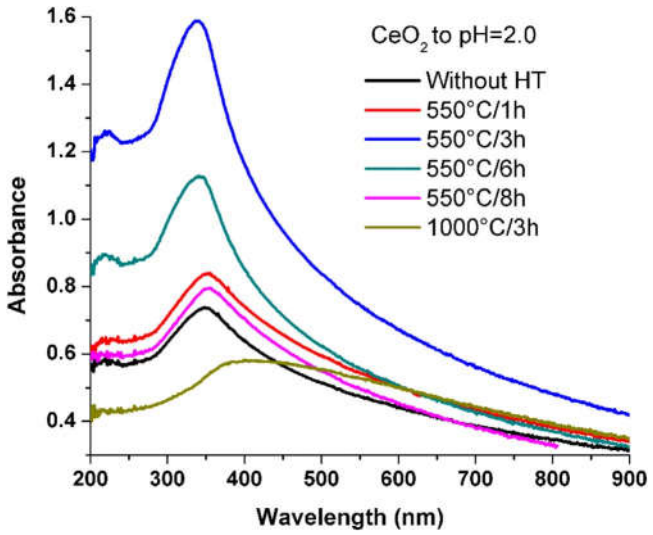


**Fig. 7.** UV–vis absorption spectra of cerium oxide powders obtained at ~pH 2 treated at 550 °C for different times.

values that coincide with those reported in the literature [64,91], but the sample treated at 1000 °C showed a shift of its absorption maximum towards the visible.

### 3.4. UV–vis diffuse reflectance results of the synthesized cerium oxides: gap energy values

Based on the results obtained using UV–vis absorption spectroscopy, it was decided to analyze in more detail the $CeO_2$ sample synthesized at pH 2.01, with different thermal treatments, using the UV–vis Diffuse Reflectance Spectroscopy (DRS) technique. The UV–vis diffuse reflectance spectra of the ceria nanoparticles of interest are shown in Fig. 8. They show little variation and all exhibit absorption peaks at 270 and 327 nm. These peaks would be generated by the charge transfer of level 2p of O to level 4f of Ce and by the 4f − 5d electronic transition in $Ce^{3+}$.

The graph of the transform of the Kubelka − Munk function was obtained from the DRS measurements (Fig. 8). The coefficient of atomic absorption (α) was calculated using the diffuse reflectance data and the Kubelka-Munk equation: $F(R) \approx \alpha \approx (1 - R)^2/2R$, where R is the percentage of light reflected. The incident photon energy (hν) and bandgap energy ($E_g$) are related through the function of the Kubelka-Munk transform[92], as mentioned above. In Fig. 8(b)–(d), the gap energy values, as well as those of the “mid-gap” states, are shown to be in agreement with those calculated using UV–vis absorption measures (Table 2): 3.9 eV and 3.4 eV respectively.

### 3.5. Transmission electron microscopy: morphology and particle size

Fig. 9 shows TEM images of the ceria obtained by the modified Pechini method, at the different pH values of synthesis. Despite the samples being subjected to ultrasound during their preparation, the images show that the particles tend to agglomerate, as is typical of nanoparticles. Moreover, the increase in the pH value of synthesis caused a reduction in the particle size, of between 10 and 20 nm, and they had a spheroidal morphology; it is necessary to emphasize that there was a greater particle size homogeneity with the cerium oxide synthesized at pH 2 (Fig. 9(b)), with particles smaller than 10 nm.

### 3.6. Proposed mechanism for the formation of ceria nanoparticles

By considering the different stages of the process carried out in this work, in order to synthesize nanoparticles of ceria, the following

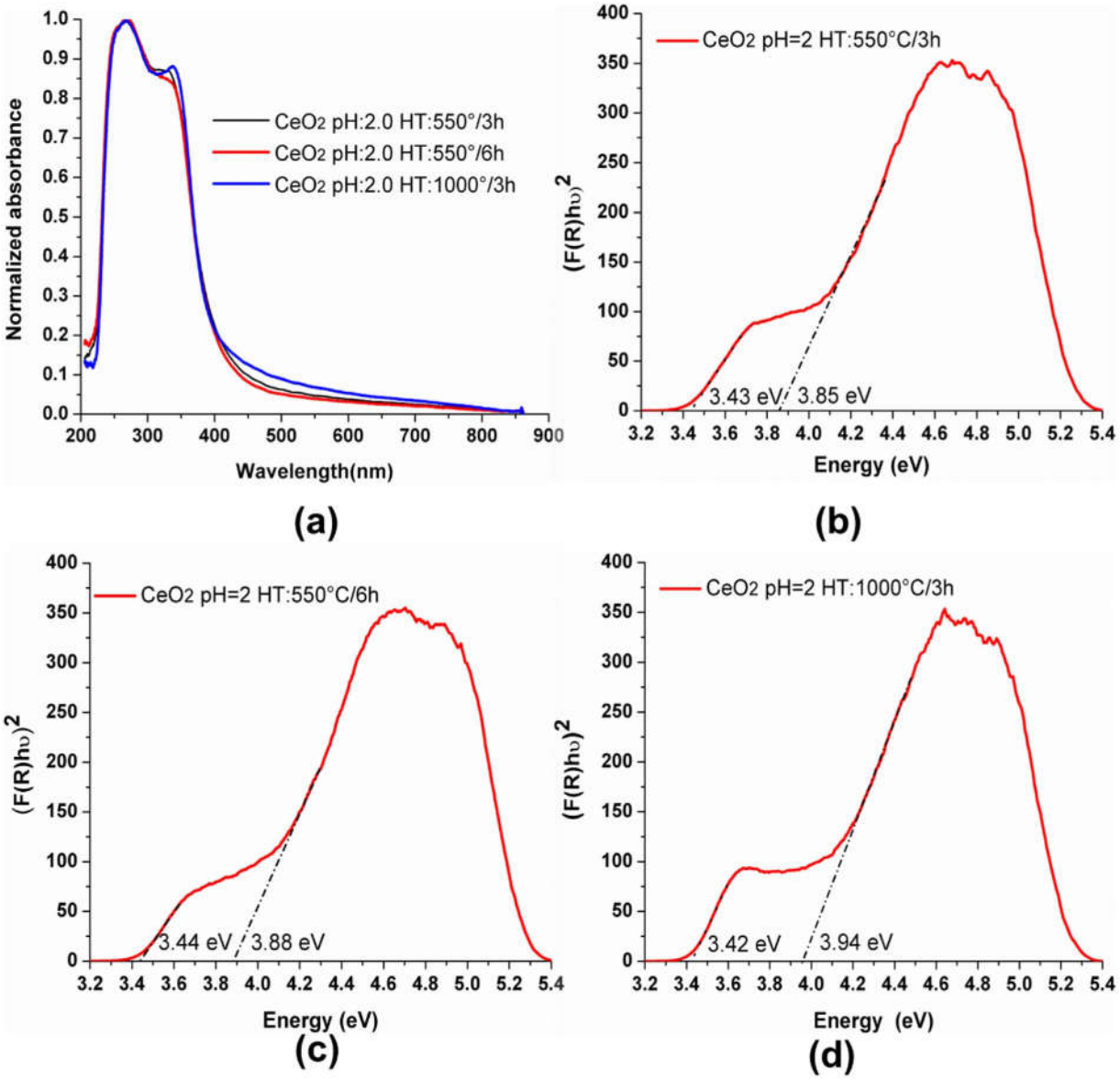


**Fig. 8.** (a) Diffuse reflectance spectra (DRS) of $CeO_2$ nanoparticles synthesized at pH 2 and heat treated at 550 °C, 3 and 6 h, and 1000 °C/3 h and graphs of the transform of the Kubelka-Munk as a function of energy, indicating the energy values obtained for energy gap Eg and mid-gap states: (b)–(d).

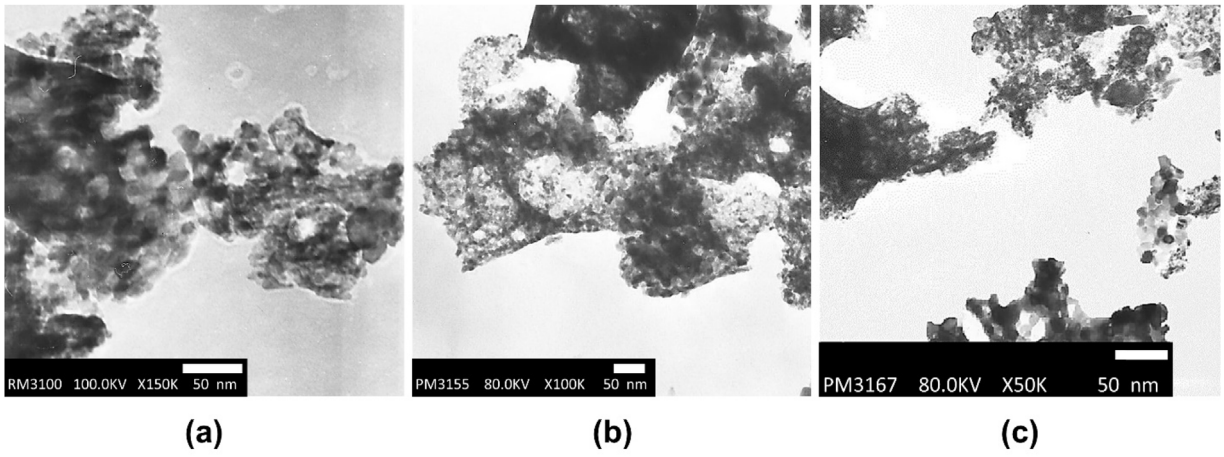


**Fig. 9.** Photos taken with TEM of ceramic powders of ceria synthesized by the modified Pechini method, at different pH values: (a) ~ 1, (b) ~2.0 and (c) 9.14, heat treated at 550 °C/3 h.

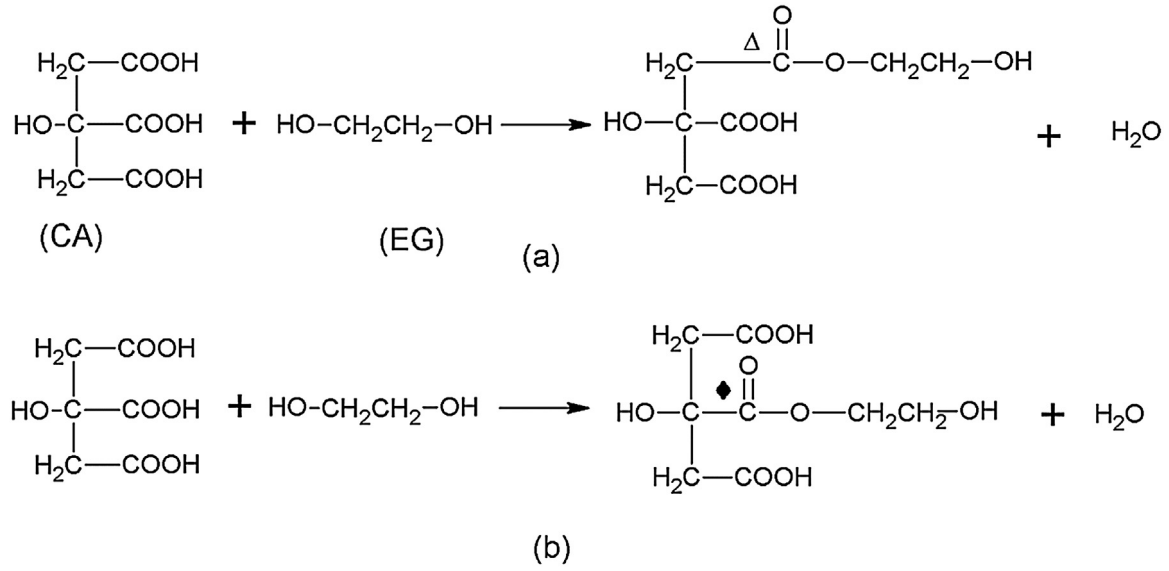


**Scheme 1.** Mixture of citric acid (CA) and ethylene glycol (EG), and dissolution of the CA in the EG.

mechanism is proposed to explain their formation. Looking at the reagents used in the process, the chemistry in the process is quite complex. The process was initiated with the mixture of citric acid (CA) and ethylene glycol (EG), at a temperature of 70 °C, which would favor the reactions indicated in Scheme 1, proposed by Kakihana in his work [93] and related to the dissolution of the CA in the EG:

During this process of dissolution, a large amount of ester products with similar structures would be formed that would favor formation of the following diester species [93] Schemes 2 and 3:

If this system is heated at temperatures ≥100 °C, successive esterification reactions will be promoted to form polyester molecules through the following reaction [93]:

Since CA has three functional carboxylic groups, branched polyester molecules can be formed. According to the theoretical calculations made by Tai and Lessing [94], the critical composition of the CA/EG mixture, at which gelation begins, is CA/EG = 2/3 (mole ratio) and not the one used in this work, CA/EG = 1/4, so it is expected that in the system there would be an excess of EG that would serve to increase the solubility of the cerium nitrate during the first stage of the process.

On dissolving the $Ce(NO_3)_3$ in the water, prior to its incorporation into the CA-EG mixture, there must have been a partial dissociation of the same, a reaction that can be expressed as:

$$Ce(NO_3)_3.6H_2O \rightarrow Ce^{3+} + 3NO_3^- + 6H_2O \quad (4)$$

with the possible presence and/or formation, in the solution, of species such as $[Ce(NO_3)_5]^{2-}$, in which the 5 bidentate nitrate groups define a trigonal bipyramid leading to tenfold coordination of cerium, and $[Ce(NO_3)_6]^{3-}$, which feature nearly regular icosahedral coordination of the metal by 12 O atoms, since the $NO_3^-$ is an inorganic counterpart and is notable for the high coordination numbers that it yields [95]. Considering the hydrolysis of $Ce^{3+}$, the possible species that could be formed in the system would be: $CeOH^{2+}$ ($LogK_{xy} = -8.3$), $Ce_2(OH)_2^{4+}$ ($LogK_{xy} < -15.5$) and $Ce_3(OH)_5^{4+}$ ($LogK_{xy} = -33.5$) [96], given the affinity of $Ce^{3+}$ for the $OH^-$.

On adding the $Ce(NO_3)_3 - H_2O$ solution to the citric acid – ethylene glycol mixture, several reactions may occur, including that of the non – dissociated $Ce(NO_3)_3$ with an excess of ethylene glycol, as indicated in Scheme 4:

Where a complex of Ce (III) would form and $HNO_3$ would be produced in the system, similar to what Xin et al. [48] suggested in their work. In this case the $Ce^{3+}$ ions can only chelate with the terminal hydroxyl groups. On the other hand, the $Ce^{3+}$ that exists in the new mixture would be able to form other chelate complexes with a structure such as indicated in Scheme 5, a molecular structure proposed by Thompson and Wiseman in their work [97]:

On adding the $NH_4OH$ to the solutionformed, to increase the pH of the system, reactions such as in Scheme 6 would be favored:

Such that for greater amounts of $NH_4OH$ added, and therefore higher pH values of the system, the oxidation reactions of Ce (III) to Ce (IV) [48] would be favored:

considering the oxygen dissolved in the solution, and the reaction:

$$Ce^{3+} + H_2O \rightarrow Ce(OH)^{3+} + H^+ + e^- \quad (5)$$

with subsequent hydrolysis to $Ce(OH)_3$, as well as hydrolysis reactions that would lead to the formation of complexes, with the water molecules and $OH^-$, of the type $[Ce(OH)_x(H_2O)_y]^{(4-x)}$ where x + y would be the coordinate number of $Ce^{4+}$.

With the subsequent addition of water to the system, to make up the 220 mL of solution, the reaction of Scheme 7 would mainly be favored and reactions such as 6 and 7 should be found [98]:

$$Ce^{4+} + xOH^- + yH_2O \rightarrow [Ce(OH)_x(H_2O)_y]^{(4-x)+} \quad (6)$$

$$[Ce(OH)_x(H_2O)_y]^{(4-x)+} + H_2O \rightarrow CeO_2.\, nH_2O + H_3O^+ \quad (7)$$

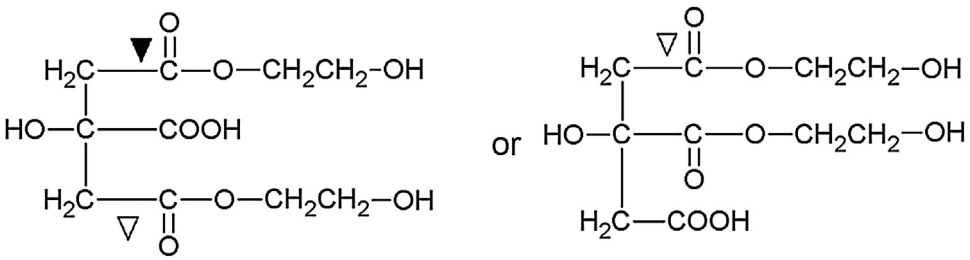


**Scheme 2.** Diester species.

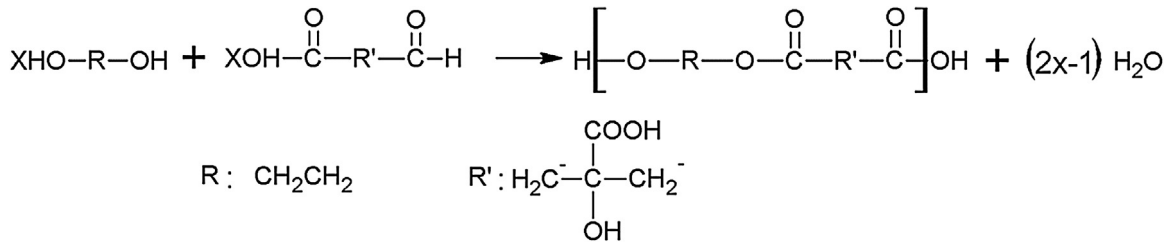

**Scheme 3.** Esterification reactions promoted to form polyester molecules.

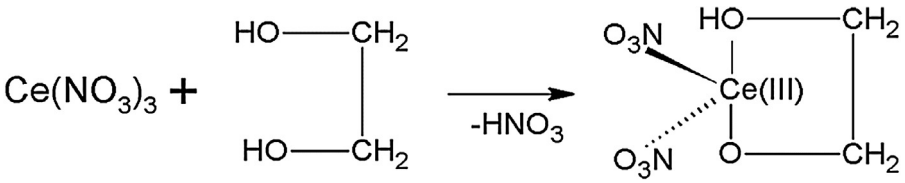

**Scheme 4.** Interaction between Non – dissociated $Ce(NO_3)_3$ with an excess of ethylene glycol.

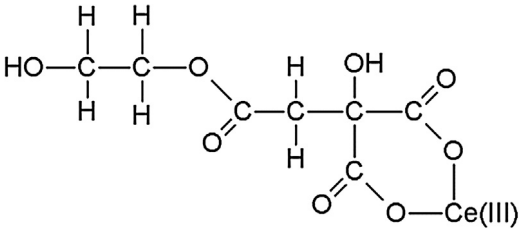

**Scheme 5.** A cerium (III) chelate complex.

Since $Ce^{3+}$ may still exist in the solution, the following reaction could also occur [49]:

$$Ce^{3+} + 4OH^{-} + xH_2O \rightarrow Ce(OH)_4.\ xH_2O \quad (8)$$

Independent of the working pH, the final mixture obtained on adding $NH_4OH$ and $H_2O$ to the $Ce(NO_3)_3$–CA – EG system was subjected to a treatment at 150 °C for 3 h, giving a resin. Finally, during the heat treatment to which the resin was subjected, at 320 °C, reactions such as the breakdown of resin would be favored [93] as well as the following ones Scheme 8:

$$Ce(OH)_4.\ xH_2O \rightarrow Ce(OH)_4 + xH_2O \quad (9a)$$

$$Ce(OH)_4 \rightarrow CeO_2 + 2H_2O \quad (9b)$$

Considering the $CO_2$ arising during the breakdown of resin, it is possible to obtain the transient intermediate precursor of cerium Ce $(OH)CO_3$ through the following reactions [75]:

$$CO_2 + H_2O \rightarrow CO_3^{2-} + 2H^{+} \quad (10)$$

$$Ce^{3+} + OH^{-} + CO_3^{2-} \rightarrow Ce(OH)CO_3 \quad (11)$$

or:

$$Ce^{3+} + NH_3.\ H_2O + CO_3^{2-} \rightarrow Ce(OH)CO_3 + NH^{4+} \quad (12)$$

such that during the calcination the following decomposition reactions of $Ce(OH)CO_3$ would be favored [99]:

$$2Ce(OH)CO_3 \rightarrow Ce_2O_3 + H_2O + 2CO_2 \quad (13)$$

$$2Ce_2O_3 + O_2 \rightarrow 4CeO_2 \quad (14)$$

where this last reaction would only occur at high oxygen concentrations, so that at the normal conditions of pressure and temperature in which the material was synthesized in this work, a mixture of sesquioxide ($Ce_2O_3$) and dioxide ($CeO_2$) would be expected as a product. In summary, considering the reactions indicated above, at the end of the synthesis process (treatment of the resin at 320 °C), the system there would be: $CeO_2$, $Ce_2O_3$ and a small organic residue as indicated by the results of IR spectroscopy (Fig. 3) and XRD (Fig. 5).

## 4. Conclusions

The methods of synthesis of ceria and its processing history may signicantly impact particle behavior. As such, the reliability and reproducibility of the production methods need to be ensured to be able to understand and predict nanoparticle behavior. In the course of this work, a reproducible and reliable synthesis methodology was developed for obtaining ceria nanoparticles at low synthesis temperatures. Considering the different stages of the process, a possible mechanism of nanoparticle formation was proposed taking account of the cerium precursor used ($Ce(NO_3)_3$), the solvents used (ethylene glycol, water and $NH_4OH$), citric acid and the various heat treatments to which the system was subjected, a mechanism that predicts the production of a mixture of sesquioxide ($Ce_2O_3$) and dioxide ($CeO_2$). The different techniques used to characterize the synthesized ceria confirmed that cerium oxide nanoparticles ( < 100 nm) were obtained and that on increasing the pH of the synthesis, a reduction in particle size resulted of between 10 and 20 nm, the particles having a spheroidal morphology. Furthermore, two energy values, 3.8 eV and 3.4 eV, were derived from the results of UV–vis absorption and diffuse reflectance spectroscopy, which could be attributed to the energy gap value (3.8 eV) and to a possible “mid-gap” (3.4 eV), where the latter would be formed by the energy states generated by defects of the ceria, within the gap, mainly by oxygen vacancies that exist in these nanoparticles and that could be formed by the $CeO_2$ to $Ce_2O_3$ reduction reaction.

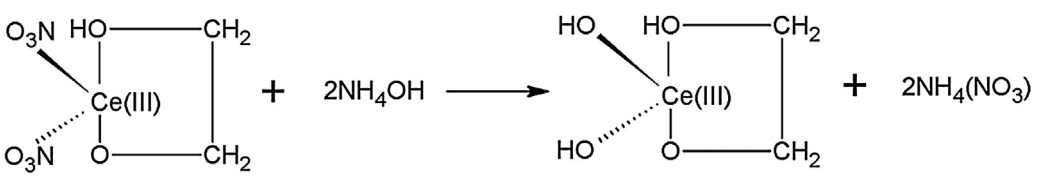

**Scheme 6.** Effect of $NH_4OH$ on a cerium intermediate complex.

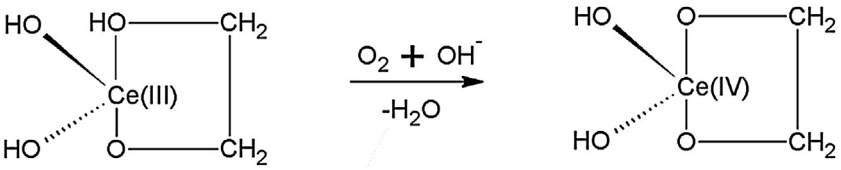


**Scheme 7.** Oxidation reactions of Ce (III) to Ce (IV) by the presence of $NH_4OH$ added.

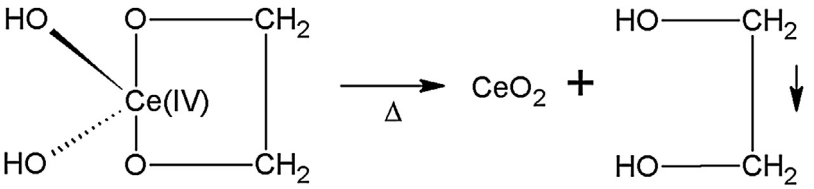


**Scheme 8.** Production of $CeO_2$ through the elimination of complexes.

## Acknowlegements

This project was funded through project ID 4162, in conjunction with the COLCIENCIAS Young Researcher program. We are grateful to the University of Cauca for making their laboratory facilities available for carrying out this work and to VRI-Unicauca for all logistical support. Particular thanks are due to chemist Caterine Daza and Dr. German Cuervo for assistance in obtaining the diffuse reflectance and UV–vis absorption spectra. We are especially grateful to Colin McLachlan for suggestions relating to the English text.

## References

[1] Inorganic Nanoparticles: Synthesis, Applications, and Perspectives, in: C. Altavilla, E. Ciliberto (Eds.), CRC Press, Boca Raton, 2011.
[2] K. Lu, Nanoparticulate Materials: Synthesis, Characterization, and Processing, John Wiley & Sons, Inc., Hoboken, NJ USA, 2012, http://dx.doi.org/10.1002/9781118408995.
[3] M.B. Gawande, A. Goswami, F.-X. Felpin, T. Asefa, X. Huang, R. Silva, X. Zou, R. Zboril, R.S. Varma, Cu and Cu-Based nanoparticles: synthesis and applications in catalysis, Chem. Rev. 116 (2016) 3722–3811, http://dx.doi.org/10.1021/acs.chemrev.5b00482.
[4] H. Abe, J. Liu, K. Ariga, Catalytic nanoarchitectonics for environmentally compatible energy generation, Mater. Today 19 (2016) 12–18, http://dx.doi.org/10.1016/j.mattod.2015.08.021.
[5] W. Park, K. Na, Advances in the synthesis and application of nanoparticles for drug delivery, Wiley Interdiscip. Rev. Nanomed. Nanobiotechnol. 7 (2015) 494–508, http://dx.doi.org/10.1002/wnan.1325.
[6] S. Stankic, S. Suman, F. Haque, J. Vidic, Pure and multi metal oxide nanoparticles: synthesis, antibacterial and cytotoxic properties, J. Nanobiotechnol. 14 (2016) 73, http://dx.doi.org/10.1186/s12951-016-0225-6.
[7] Nanoscale Materials in Chemistry, in: K.J. Klabunde, R.M. Richards (Eds.), John Wiley & Sons, Inc., Hoboken, NJ, USA, 2009, http://dx.doi.org/10.1002/9780470523674.
[8] F. Charbgoo, M. Bin Ahmad, M. Darroudi, Cerium oxide nanoparticles: green synthesis and biological applications, Int. J. Nanomed. 12 (2017) 1401–1413, http://dx.doi.org/10.2147/IJN.S124855.
[9] H.L. Nguyen, H.N. Nguyen, H.H. Nguyen, M.Q. Luu, M.H. Nguyen, Nanoparticles: synthesis and applications in life science and environmental technology, Adv. Nat. Sci. Nanosci. Nanotechnol. 6 (2015) 15008, http://dx.doi.org/10.1088/2043-6262/6/1/015008.
[10] G. Adachi, N. Imanaka, The binary rare earth oxides, Chem. Rev. 98 (1998) 1479–1514, http://dx.doi.org/10.1021/cr940055h.
[11] S. Gangopadhyay, D.D. Frolov, A.E. Masunov, S. Seal, Structure and properties of cerium oxides in bulk and nanoparticulate forms, J. Alloys Compd. 584 (2014) 199–208, http://dx.doi.org/10.1016/j.jallcom.2013.09.013.
[12] C. Sun, L. Hong, L. Chen, Nanostructured ceria-based materials: synthesis, properties, and applications, Energy Environ. Sci. 5 (2012) 8475–8505, http://dx.doi.org/10.1039/c2ee22310d.
[13] B. Choudhury, A. Choudhury, $Ce^{3+}$ and oxygen vacancy mediated tuning of structural and optical properties of $CeO_2$ nanoparticles, Mater. Chem. Phys. 131 (2012) 666–671, http://dx.doi.org/10.1016/j.matchemphys.2011.10.032.
[14] N.V. Skorodumova, S.I. Simak, B.I. Lundqvist, I.A. Abrikosov, B. Johansson, Quantum origin of the oxygen storage capability of ceria, Phys. Rev. Lett. 89 (2002) 166601, http://dx.doi.org/10.1103/PhysRevLett.89.166601.
[15] V.G. Brauer, H. Gradinger, Über heterotype mischphasen bei seltenerdoxyden. II. die oxydsysteme des cers und des praseodyms, Zeitschrift Für Anorg Und Allg. Chemie. 277 (1954) 89–95, http://dx.doi.org/10.1002/zaac.19542770110.
[16] D.J.M. Bevan, Ordered intermediate phases in the system $CeO_2$-$Ce_2O_3$, J. Inorg. Nucl. Chem. 1 (1955) 49–59, http://dx.doi.org/10.1016/0022-1902(55)80067-X.
[17] D. Marrocchelli, S.R. Bishop, H.L. Tuller, B. Yildiz, Understanding chemical expansion in non-stoichiometric oxides: ceria and zirconia case studies, Adv. Funct. Mater. 22 (2012) 1958–1965, http://dx.doi.org/10.1002/adfm.201102648.
[18] N.J. Lawrence, J.R. Brewer, L. Wang, T.S. Wu, J. Wells-Kingsbury, M.M. Ihrig, G. Wang, Y.L. Soo, W.N. Mei, C.L. Cheung, Defect engineering in cubic cerium oxide nanostructures for catalytic oxidation, Nano Lett. 11 (2011) 2666–2671, http://dx.doi.org/10.1021/nl200722z.
[19] R.J. Gorte, Ceria in catalysis: from automotive applications to the water-gas shift reaction, AlChE J. 56 (2010) 1126–1135, http://dx.doi.org/10.1002/aic.12234.
[20] J. Paier, C. Penschke, J. Sauer, Oxygen defects and surface chemistry of ceria: quantum chemical studies compared to experiment, Chem. Rev. 113 (2013) 3949–3985, http://dx.doi.org/10.1021/cr3004949.
[21] A. Trovarelli, P. Fornasiero, Catalysis by ceria and related materials, Catalytic Science Series, 2nd ed., Imperial College Press, Italy, 2005, http://dx.doi.org/10.1016/j.cattod.2004.12.016.
[22] J.F. Jerratsch, X. Shao, N. Nilius, H.J. Freund, C. Popa, M.V. Ganduglia-Pirovano, A.M. Burow, J. Sauer, Electron localization in defective ceria films: a study with scanning-tunneling microscopy and density-functional theory, Phys. Rev. Lett. 106 (2011) 246801, http://dx.doi.org/10.1103/PhysRevLett.106.246801.
[23] S. Hull, S.T. Norberg, I. Ahmed, S.G. Eriksson, D. Marrocchelli, P.A. Madden, Oxygen vacancy ordering within anion-deficient Ceria, J. Solid State Chem. 182 (2009) 2815–2821, http://dx.doi.org/10.1016/j.jssc.2009.07.044.
[24] Z. Wu, S.H. Overbury, Catalysis by Materials with Well-Defined Structures, Elsevier, Oxford, 2015.
[25] G.A. Deluga, J.R. Salge, L.D. Schmidt, X.E. Verykios, Renewable hydrogen from ethanol by autothermal reforming, Science 303 (2004) 993–997, http://dx.doi.org/10.1126/science.1093045.
[26] K. Otsuka, T. Ushiyama, I. Yamanaka, Partial oxidation of methane using the redox of cerium oxide, Chem. Lett. 22 (1993) 1517–1520, http://dx.doi.org/10.1246/Cl.1993.1517.
[27] S. Park, J.M. Vohs, R.J. Gorte, Direct oxidation of hydrocarbons in a solid-oxide fuel cell, Nature 404 (2000) 265–267, http://dx.doi.org/10.1038/35005040.
[28] S. Tsunekawa, R. Sivamohan, T. Ohsuna, H. Takahashi, K. Tohji, Ultraviolet absorption spectra of $CeO_2$ nano-particles, Mater. Sci. Forum. 315–317 (1999) 439–445, http://dx.doi.org/10.4028/www.scientific.net/MSF.315-317.439.
[29] N.M. Zholobak, V.K. Ivanov, A.B. Shcherbakov, Interaction of nanoceria with microorganisms, in: A.M. Grumezescu (Ed.), Nanobiomaterials Antimicrob. Ther. Elsevier Inc., Bucharest, 2016, pp. 419–450 , http://dx.doi.org/10.1016/B978-0-323-42864-4.00012-9.
[30] S. Das, J.M. Dowding, K.E. Klump, J.F. McGinnis, W. Self, S. Seal, Cerium oxide nanoparticles: applications and prospects in nanomedicine, Nanomedicine 8 (2013) 1483–1508, http://dx.doi.org/10.2217/nnm.13.133.
[31] P. Jasinski, T. Suzuki, H.U. Anderson, Nanocrystalline undoped ceria oxygen sensor, Sens. Actuators B Chem. 95 (2003) 73–77, http://dx.doi.org/10.1016/S0925-4005(03)00407-6.
[32] I. Celardo, J.Z. Pedersen, E. Traversa, L. Ghibelli, Pharmacological potential of cerium oxide nanoparticles, Nanoscale 3 (2011) 1411–1420, http://dx.doi.org/10.1039/c0nr00875c.
[33] H.R. Pouretedal, A. Kadkhodaie, Synthetic $CeO_2$ nanoparticle catalysis of methylene blue photodegradation: kinetics and mechanism, Chin. J. Catal. 31 (2010) 1328–1334, http://dx.doi.org/10.1016/S1872-2067(10)60121-0.
[34] A. Bumajdad, J. Eastoe, A. Mathew, Cerium oxide nanoparticles prepared in self-assembled systems, Adv. Colloid Interface Sci. 147-148 (2009) 56–66, http://dx.doi.org/10.1016/j.cis.2008.10.004.
[35] K.S. Lin, S. Chowdhury, Synthesis, characterization, and application of 1-D cerium oxide nanomaterials: a review, Int. J. Mol. Sci. 11 (2010) 3226–3251, http://dx.doi.org/10.3390/ijms11093226.
[36] M. Hirano, M. Inagaki, Preparation of monodispersed cerium(IV) oxide particles by thermal hydrolysis: influence of the presence of urea and Gd doping on their morphology and growth, J. Mater. Chem. 10 (2000) 473–477, http://dx.doi.org/10.1039/A907510K.
[37] M. Kamruddin, P.K. Ajikumar, R. Nithya, A.K. Tyagi, B. Raj, Synthesis of nanocrystalline ceria by thermal decomposition and soft-chemistry methods, Scr. Mater. 50 (2004) 417–422, http://dx.doi.org/10.1016/j.scriptamat.2003.11.010.
[38] C. Laberty-Robert, J.W. Long, E.M. Lucas, K.A. Pettigrew, R.M. Stroud, M.S. Doescher, D.R. Rolison, Sol-gel-derived ceria nanoarchitectures: synthesis, characterization, and electrical properties, Chem. Mater. 18 (2006) 50–58, http://dx.doi.org/10.1021/cm051385t.

[39] R.D. Purohit, B.P. Sharma, K.T. Pillai, A.K. Tyagi, Ultrafine ceria powders via glycine-nitrate combustion, Mater. Res. Bull. 36 (2001) 2711–2721, http://dx.doi.org/10.1016/S0025-5408(01)00762-0.
[40] M. Hirano, E. Kato, Hydrothermal synthesis of cerium(IV) oxide powders, J. Am. Ceram. Soc. 82 (1999) 786–788, http://dx.doi.org/10.1111/j.1151-2916.1996.tb07943.x.
[41] C. Sun, L. Chen, Controllable synthesis of shuttle-shaped ceria and its catalytic properties for CO oxidation, Eur. J. Inorg. Chem. 2009 (2009) 3883–3887, http://dx.doi.org/10.1002/ejic.200900362.
[42] Y. He, B. Yang, G. Cheng, Controlled synthesis of $CeO_2$ nanoparticles from the coupling route of homogenous precipitation with microemulsion, Mater. Lett. 57 (2003) 1880–1884, http://dx.doi.org/10.1016/S0167-577X(02)01093-5.
[43] L. Yin, Y. Wang, G. Pang, Y. Koltypin, A. Gedanken, Sonochemical synthesis of cerium oxide nanoparticles-Effect of additives and quantum size effect, J. Colloid Interface Sci. 246 (2002) 78–84, http://dx.doi.org/10.1006/jcis.2001.8047.
[44] Y.X. Li, X.Z. Zhou, Y. Wang, X.Z. You, Preparation of nano-sized $CeO_2$ by mechanochemical reaction of cerium carbonate with sodium hydroxide, Mater. Lett. 58 (2003) 245–249, http://dx.doi.org/10.1016/S0167-577X(03)00454-3.
[45] H.-J. Choi, J. Moon, H.-B. Shim, K.-S. Han, E.-G. Lee, K.-D. Jung, Preparation of nanocrystalline $CeO_2$ by the precipitation method and its improved methane oxidation activity, J. Am. Ceram. Soc. 89 (2006) 343–345, http://dx.doi.org/10.1111/j.1551-2916.2005.00670.x.
[46] I.T. Liu, M.H. Hon, L.G. Teoh, Structure and optical properties of $CeO_2$ nanoparticles synthesized by precipitation, J. Electron. Mater. 42 (2013) 2536–2541, http://dx.doi.org/10.1007/s11664-013-2617-9.
[47] S. Deshpande, S. Patil, S.V. Kuchibhatla, S. Seal, Size dependency variation in lattice parameter and valency states in nanocrystalline cerium oxide, Appl. Phys. Lett. 87 (2005) 133113, http://dx.doi.org/10.1063/1.2061873.
[48] Y. Xin, X. Yang, P. Jiang, Z. Zhang, Z. Wang, Y. Zhang, Synthesis of $CeO_2$-based quantum dots through a polyol-hydrolysis method for fuel-borne catalysts, ChemCatChem 3 (2011) 1772–1778, http://dx.doi.org/10.1002/cctc.201100179.
[49] J.J. Ketzial, A.S. Nesaraj, Synthesis of $CeO_2$ nanoparticles by chemical precipitation and the effect of a surfactant on the distribution of particle sizes, J. Ceram. Process. Res. 12 (2011) 74–79.
[50] F. Heidari, A. Irankhah, Effect of surfactants and digestion time on nano crystalline cerium oxide characteristics synthesized by differential precipitation, Ceram. Int. 40 (2014) 12655–12660, http://dx.doi.org/10.1016/j.ceramint.2014.04.112.
[51] H.Y. Chang, H.I. Chen, Morphological evolution for $CeO_2$ nanoparticles synthesized by precipitation technique, J. Cryst. Growth 283 (2005) 457–468, http://dx.doi.org/10.1016/j.jcrysgro.2005.06.002.
[52] V. Morris, P.G. Fleming, J.D. Holmes, M.A. Morris, Comparison of the preparation of cerium oxide nanocrystallites by forward (base to acid) and reverse (acid to base) precipitation, Chem. Eng. Sci. 91 (2013) 102–110, http://dx.doi.org/10.1016/j.ces.2013.01.016.
[53] H.I. Chen, H.Y. Chang, Homogeneous precipitation of cerium dioxide nanoparticles in alcohol/water mixed solvents, Colloids Surfaces A Physicochem Eng. Asp. 242 (2004) 61–69, http://dx.doi.org/10.1016/j.colsurfa.2004.04.056.
[54] D. Zhang, F. Niu, H. Li, L. Shi, J. Fang, Uniform ceria nanospheres: solvothermal synthesis, formation mechanism, size-control and catalytic activity, Powder Technol. 207 (2011) 35–41, http://dx.doi.org/10.1016/j.powtec.2010.10.007.
[55] A.S. Karakoti, P. Munusamy, K. Hostetler, V. Kodali, S. Kuchibhatla, G. Orr, J.G. Pounds, J.G. Teeguarden, B.D. Thrall, D.R. Baer, Preparation and characterization challenges to understanding environmental and biological impacts of ceria nanoparticles, Surf. Interface Anal. 44 (2012) 882–889, http://dx.doi.org/10.1002/sia.5006.
[56] S.H. Joo, D. Zhao, Environmental dynamics of metal oxide nanoparticles in heterogeneous systems: a review, J. Hazard. Mater. 322 (2017) 29–47, http://dx.doi.org/10.1016/j.jhazmat.2016.02.068.
[57] A. Nemmar, J.A. Holme, I. Rosas, P.E. Schwarze, E. Alfaro-Moreno, Recent advances in particulate matter and nanoparticle toxicology: a review of the in vivo and in vitro studies, BioMed Res. Int. 2013 (2013) 279371, http://dx.doi.org/10.1155/2013/279371.
[58] R.A. Yokel, S. Hussain, S. Garantziotis, P. Demokritou, V. Castranova, F.R. Cassee, The yin: an adverse health perspective of nanoceria: uptake, distribution, accumulation, and mechanisms of its toxicity, Environ. Sci. Nano 1 (2014) 406–428, http://dx.doi.org/10.1039/C4EN00039K.
[59] D. Schubert, R. Dargusch, J. Raitano, S.-W. Chan, Cerium and yttrium oxide nanoparticles are neuroprotective, Biochem. Biophys. Res. Commun. 342 (2006) 86–91, http://dx.doi.org/10.1016/j.bbrc.2006.01.129.
[60] A. Kumar, S. Das, P. Munusamy, W. Self, D.R. Baer, D.C. Sayle, S. Seal, J.I. Zink, A.E. Nel, S. Das, S. Seal, S. Seal, B.W. Eichhorn, P. Mulvaney, C.B. Murray, A.L. Rogach, P.S. Weiss, I. Willner, W.J. Parak, Behavior of nanoceria in biologically-relevant environments, Environ. Sci. Nano 1 (2014) 516–532, http://dx.doi.org/10.1039/C4EN00052H.
[61] K. Reed, A. Cormack, A. Kulkarni, M. Mayton, D. Sayle, F. Klaessig, B. Stadler, Exploring the properties and applications of nanoceria: is there still plenty of room at the bottom? Environ Sci. Nano 1 (2014) 390–405, http://dx.doi.org/10.1039/C4EN00079J.
[62] Q. Yuan, H. Duan, L. Li, L. Sun, Y. Zhang, C. Yan, Controlled synthesis and assembly of ceria-based nanomaterials, J. Colloid Interface Sci. 335 (2009) 151–167, http://dx.doi.org/10.1016/j.jcis.2009.04.007.
[63] W.P. Hsu, L. Rönnquist, E. Matijevic, Preparation and properties of monodispersed colloidal particles of lanthanide compounds. 2. Cerium(IV), Langmuir 4 (1988) 31–37, http://dx.doi.org/10.1021/la00079a005.
[64] L. Truffault, M.-T. Ta, T. Devers, K. Konstantinov, C. Simmonard, C. Andreazza, I.P. Nevirkovets, A. Pineau, O. Veron, J.-P. Blondeau, Application of nanostructured Ca doped $CeO_2$ for ultraviolet filtration, Mater. Res. Bull. 45 (2010) 527–535, http://dx.doi.org/10.1016/j.materresbull.2010.02.008.
[65] R.A. Smith, Semiconductors, 2nd ed., Cambridge University Press, Cambridge, 1978.
[66] P. Kubelka, F. Munk, Ein Beitrag zur Optik der Farbanstriche, Zeitschrift Für Tech. Phys. 12 (1931) 593–601.
[67] M. Mogensen, N.M. Sammes, G.A. Tompsett, Physical, chemical and electrochemical properties of pure and doped ceria, Solid State Ionics 129 (2000) 63–94, http://dx.doi.org/10.1016/S0167-2738(99)00318-5.
[68] G.V. Samsonov, The Oxide Handbook, Springer, US, Boston, MA, 1973, http://dx.doi.org/10.1007/978-1-4615-9597-7.
[69] O.T. Soerensen, Nonstoichiometric Oxides, Materials Science Serie, Academic Press Inc, London, 1981, http://dx.doi.org/10.1016/B978-0-12-655280-5.50001-8.
[70] T. Wang, D.C. Sun, Preparation and characterization of nanometer-scale powders ceria by electrochemical deposition method, Mater. Res. Bull. 43 (2008) 1754–1760, http://dx.doi.org/10.1016/j.materresbull.2007.07.008.
[71] D. Andreescu, E. Matijević, D.V. Goia, Formation of uniform colloidal ceria in polyol, Colloids Surfaces A Physicochem. Eng. Asp. 291 (2006) 93–100, http://dx.doi.org/10.1016/j.colsurfa.2006.05.006.
[72] J. Liu, Z. Zhao, J. Wang, C. Xu, A. Duan, G. Jiang, Q. Yang, The highly active catalysts of nanometric $CeO_2$-supported cobalt oxides for soot combustion, Appl. Catal. B Environ. 84 (2008) 185–195, http://dx.doi.org/10.1016/j.apcatb.2008.03.017.
[73] S.P. Ray, D.E. Cox, Neutron diffraction determination of the crystal structure of $Ce_7O_{12}$, J. Solid State Chem. 15 (1975) 333–343, http://dx.doi.org/10.1016/0022-4596(75)90289-3.
[74] S. Phoka, P. Laokul, E. Swatsitang, V. Promarak, S. Seraphin, S. Maensiri, Synthesis, structural and optical properties of $CeO_2$ nanoparticles synthesized by a simple polyvinyl pyrrolidone (PVP) solution route, Mater. Chem. Phys. 115 (2009) 423–428, http://dx.doi.org/10.1016/j.matchemphys.2008.12.031.
[75] S. Wang, F. Gu, C. Li, H. Cao, Shape-controlled synthesis of $CeOHCO_3$ and $CeO_2$ microstructures, J. Cryst. Growth 307 (2007) 386–394, http://dx.doi.org/10.1016/j.jcrysgro.2007.06.025.
[76] A. Vantomme, Z.Y. Yuan, G. Du, B.L. Su, Surfactant-assisted large-scale preparation of crystalline $CeO_2$ nanorods, Langmuir 21 (2005) 1132–1135, http://dx.doi.org/10.1021/la047751p.
[77] S. Chen, T. Cao, Y. Gao, D. Li, F. Xiong, W. Huang, Probing surface structures of $CeO_2$, $TiO_2$, and $Cu_2O$ nanocrystals with CO and $CO_2$ chemisorption, J. Phys. Chem. C 120 (2016) 21472–21485, http://dx.doi.org/10.1021/acs.jpcc.6b06158.
[78] L.H. Little, Infrared Spectra of Adsorbed Species, Academic Press, London-New York, 1966https://www.amazon.com/Infrared-Spectra-Adsorbed-Species-Little/dp/0124521509.
[79] R. Rajendran, L.K. Shrestha, K. Minami, M. Subramanian, R. Jayavel, K. Ariga, Dimensionally integrated nanoarchitectonics for a novel composite from 0D, 1D, and 2D nanomaterials: RGO/CNT/$CeO_2$ ternary nanocomposites with electrochemical performance, J. Mater. Chem. A 2 (2014) 18480–18487, http://dx.doi.org/10.1039/C4TA03996C.
[80] M.L. Dos Santos, R.C. Lima, C.S. Riccardi, R.L. Tranquilin, P.R. Bueno, J.A. Varela, E. Longo, Preparation and characterization of ceria nanospheres by microwave-hydrothermal method, Mater. Lett. 62 (2008) 4509–4511, http://dx.doi.org/10.1016/j.matlet.2008.08.011.
[81] M. Zawadzki, Preparation and characterization of ceria nanoparticles by microwave-assisted solvothermal process, J. Alloys Compd. 454 (2008) 347–351, http://dx.doi.org/10.1016/j.jallcom.2006.12.078.
[82] R. Suresh, V. Ponnuswamy, R. Mariappan, Effect of annealing temperature on the microstructural, optical and electrical properties of $CeO_2$ nanoparticles by chemical precipitation method, Appl. Surf. Sci. 273 (2013) 457–464, http://dx.doi.org/10.1016/j.apsusc.2013.02.062.
[83] M. Nolan, S. Grigoleit, D.C. Sayle, S.C. Parker, G.W. Watson, Density functional theory studies of the structure and electronic structure of pure and defective low index surfaces of ceria, Surf. Sci. 576 (2005) 217–229, http://dx.doi.org/10.1016/j.susc.2004.12.016.
[84] N.V. Skorodumova, R. Ahuja, S.I. Simak, I.A. Abrikosov, B. Johansson, B.I. Lundqvist, Electronic, bonding, and optical properties of $CeO_2$ and $Ce_3$ from first principles, Phys. Rev. B 64 (2001) 115108, http://dx.doi.org/10.1103/PhysRevB.64.115108.
[85] F. Le Normand, J. El Fallah, L. Hilaire, P. Légaré, A. Kotani, J.C. Parlebas, Photoemission on 3d core levels of cerium: an experimental and theoretical investigation of the reduction of cerium dioxide, Solid State Commun. 71 (1989) 885–889, http://dx.doi.org/10.1016/0038-1098(89)90555-3.
[86] A. Fujimori, Mixed-valent ground state of $CeO_2$, Phys. Rev. B 28 (1983) 2281–2283.
[87] E. Wuilloud, B. Delley, W.-D. Schneider, Y. Baer, Spectroscopic evidence for localized and extended f-symmetry states in $CeO_2$, Phys. Rev. Lett. 53 (1984) 202–205, http://dx.doi.org/10.1103/PhysRevLett.53.202.
[88] P. Nagpal, V.I. Klimov, Role of mid-gap states in charge transport and photoconductivity in semiconductor nanocrystal films, Nat. Commun. 2 (2011) 486, http://dx.doi.org/10.1038/ncomms1492.
[89] H. Yaghoubi, Z. Li, Y. Chen, H.T. Ngo, V.R. Bhethanabotla, B. Joseph, S. Ma, R. Schlaf, A. Takshi, Toward a visible light-driven photocatalyst: the effect of midgap-states-induced energy gap of undoped $TiO_2$ nanoparticles, ACS Catal. 5 (2015) 327–335, http://dx.doi.org/10.1021/cs501539q.
[90] R. Verma, S.K. Samdarshi, S. Bojja, S. Paul, B. Choudhury, A novel thermo-photocatalyst of mixed-phase cerium oxide ($CeO_2$/$Ce_2O_3$) homocomposite nanostructure: role of interface and oxygen vacancies, Sol. Energy Mater. Sol. Cells 141 (2015) 414–422, http://dx.doi.org/10.1016/j.solmat.2015.06.027.
[91] M. Chelliah, J.B.B. Rayappan, U.M. Krishnan, Synthesis and characterization of

cerium oxide nanoparticles by hydroxide mediated approach, J. Appl. Sci. 12 (2012) 1734–1737, http://dx.doi.org/10.3923/jas.2012.1734.1737.
[92] A. Escobedo Morales, E. Sánchez Mora, U. Pal, Use of diffuse reflectance spectroscopy for optical characterization of un-supported nanostructures, Rev. Mex. Física S 53 (2007) 18–22 http://www.redalyc.org/articulo.oa?id=57028299004.
[93] M. Kakihana, Sol-gel preparation of high temperature superconducting oxides, J. Sol-Gel Sci. Technol. 6 (1996) 7–55, http://dx.doi.org/10.1007/BF00402588.
[94] L. Tai, P.A. Lessing, Modified resin-intermediate processing of perovskite powders: part I. Optimization of polymeric precursors, J. Mater. Res. 7 (1992) 502–510, http://dx.doi.org/10.1557/JMR.1992.0502.
[95] N.N. Greenwood, A. Earnshaw, The Lanthanide Elements (Z = 58–71), second ed., Butterworth-Heinemann, Oxford, 1997, pp. 1227–1249 (Chem. Elem.).
[96] C.F. Baes, R.S. Mesmer, The Hydrolysis of Cations, Wiley, New York, 1976, http://dx.doi.org/10.1002/bbpc.19770810252.
[97] M.S. Thompson, G.H. Wiseman, Synthesis and microstructure of gel-derived varistor precursor powders, Ceram. Int. 15 (1989) 281–288, http://dx.doi.org/10.1016/0272-8842(89)90030-8.
[98] H. Wang, J.-J. Zhu, J. Zhu, X. Liao, S. Xu, T. Ding, H. Chen, Preparation of nanocrystalline ceria particles by sonochemical and microwave assisted heating methods, Phys. Chem. Chem. Phys. 4 (2002) 3794–3799, http://dx.doi.org/10.1039/b201394k.
[99] Y. Chen, C. Qiu, C. Chen, X. Fan, S. Xu, W. Guo, Z. Wang, Facile synthesis of ceria nanospheres by Ce(OH)CO3 precursors, Mater. Lett. 122 (2014) 90–93, http://dx.doi.org/10.1016/j.matlet.2014.01.178.